For the approximate solution, we set $v = \phi\mathbf{v}$, $u = \psi\mathbf{u}$, $\eta = \psi\boldsymbol{\eta} = \bar{\psi}\mathbf{v}$, and $\lambda = \gamma(x)\boldsymbol{\lambda}$. Then, $\pi(\mathbf{u}, \mathbf{v}, \boldsymbol{\eta}, \boldsymbol{\lambda})$ assumes a stationary value for each finite element when the following local equations are satisfied:

$$\int_0^h \{EI\boldsymbol{\phi}''^T\boldsymbol{\phi}''\mathbf{v} - q\boldsymbol{\phi}^T + \boldsymbol{\phi}^T\gamma\boldsymbol{\lambda}\}\,dx = 0 \tag{9a}$$

$$\int_0^h \left\{EA\boldsymbol{\psi}'^T\boldsymbol{\psi}'\boldsymbol{\eta}\boldsymbol{\psi}'\mathbf{u} + \frac{EA}{2}\boldsymbol{\psi}'^T\boldsymbol{\psi}'\boldsymbol{\eta}\boldsymbol{\eta}^T\boldsymbol{\psi}'^T\boldsymbol{\psi}'\boldsymbol{\eta} - \boldsymbol{\psi}^T\gamma\boldsymbol{\lambda}\right\} dx = 0 \tag{9b}$$

$$\int_0^h \left\{EA\boldsymbol{\psi}'^T\boldsymbol{\psi}'\mathbf{u} + \frac{EA}{2}\boldsymbol{\psi}'^T\boldsymbol{\eta}^T\boldsymbol{\psi}'^T\boldsymbol{\psi}'\boldsymbol{\eta}\right\} dx = 0 \tag{9c}$$

$$\int_0^h \gamma^T(\boldsymbol{\phi}\mathbf{v} - \boldsymbol{\psi}\boldsymbol{\eta})\,dx = 0 \tag{9d}$$

Comparing Eqs. (9) and (6), we see that the latter can be obtained from Eq. (9) only by approximately satisfying the local constraint condition (9d). Since $\boldsymbol{\psi}(x)$ and $\boldsymbol{\phi}(x)$ are known in terms of h via Eq. (3), we can calculate immediately

$$\int_0^h \gamma^T(\boldsymbol{\phi}\mathbf{v} - \boldsymbol{\psi}\boldsymbol{\eta})\,dx = h/2\begin{Bmatrix}(v_1-\eta_1)+(v_2-\eta_2)\\(v_1-\eta_1)+(v_2-\eta_2)\end{Bmatrix} + \begin{Bmatrix}O(h^2)\\O(h^2)\end{Bmatrix} \tag{10}$$

assuming $\gamma(x) = [1, 1]$. Hence, introduction of Eq. (10) into Eq. (9) yields Eq. (6) plus terms of order h^2. However, this process only serves to interpret Eq. (6); it still remains to be shown that Eq. (6) is an acceptable approximation.

Convergence

Let u^*, v^*, η^*, and λ^* be the exact functions providing a stationary value of $\pi(u, v, \eta, \lambda)$, let U^*, V^*, and H^* be the finite element solution, and let $\tilde{U}$, $\tilde{V}$, and $\tilde{H}$ be finite element interpolations. Let u, v, η, and λ be arbitrary values of the indicated variables. Then a simple calculation leads to the relation

$$\begin{aligned}\pi(u,v,\eta,\lambda) = \pi(u^*,v^*,\eta^*,\lambda^*) + \int_0^L \Big\{&\frac{EA}{2}(u'-u^{*\prime})^2 + \\ &(EI/2)(v''-v^{*\prime\prime})^2 - (P/2)(\eta'-\eta^{*\prime})^2 + (EA/2)\eta^{*\prime 2}(\eta'-\eta^{*\prime})^2 + \\ &EA\eta^{*\prime}(\eta'-\eta^{*\prime})(u'-u^{*\prime}) + (EA/2)(u'-u^{*\prime})(\eta'-\eta^{*\prime})^2 + \\ &(EA/2)\eta^{*\prime}(\eta'-\eta^{*\prime})^3 + (EA/8)(\eta'-\eta^{*\prime})^4 + (\lambda-\lambda^*)(v-v^*) - \\ &(\lambda-\lambda^*)(\eta-n^*)\Big\}\,dx\end{aligned} \tag{11}$$

Among possible displacement fields the deformed beam can assume are those for which the terms appearing in the preceding integral are positive. This being the case, we can assert that

$$|\varepsilon| \leqq |\pi(\tilde{U}, \tilde{V}, \tilde{H}, \lambda^*) - \pi(u^*, v^*, \eta^*, \lambda^*)| \tag{12}$$

where ε is the error in energy

$$\varepsilon = \pi(U^*, V^*, H^*, \lambda^*) - \pi(u^*, v^*, \eta^*, \lambda^*) \tag{13}$$

Assuming that the slope is bounded (i.e. $|\eta^{*\prime}| < M_0 < \infty$), we can use the mean value theorem, and the Schwarz's inequality, to extract from Eqs. (11) and (12) the following inequality:

$$\begin{aligned}|\varepsilon| \leqq\ &(EA/2)\|\tilde{U}'-u^{*\prime}\|^2_{L_2(0,L)} + (EI/2)\|\tilde{V}''-v^{*\prime\prime}\|^2_{L_2(0,L)} - \\ &(P/2)\|\tilde{H}'-\eta^{*\prime}\|^2_{L_2(0,L)} + (EA/2)M_0{}^2\|\tilde{H}'-\eta^{*\prime}\|^2_{L_2(0,L)} + \\ &EAM_0\|\tilde{H}'-\eta^{*\prime}\|_{L_2(0,L)}\|\tilde{U}'-u^{*\prime}\|_{L_2(0,L)} + \\ &(EA/2)\|\tilde{U}'-u^{*\prime}\|_{L_\infty(0,L)}\|\tilde{H}'-\eta^{*\prime}\|^2_{L_2(0,L)} + \\ &(EA/2)M_0\|\tilde{H}'-\eta^{*\prime}\|_{L_\infty(0,L)}\|\tilde{H}'-\eta^{*\prime}\|^2_{L_2(0,L)} + \\ &(EA/8)\|\tilde{H}'-\eta^{*\prime}\|^2_{L_\infty(0,L)}\|\tilde{H}'-\eta^{*\prime}\|^2_{L_2(0,L)}\end{aligned} \tag{14}$$

Introducing Eq. (7) with $k = 1$ for approximations of u and η, $k = 3$ for those of v we obtain

$$\begin{aligned}|\varepsilon| \leqq\ &(EA/2)K_1h^2 + (EI/2)K_2h^4 - (P/2)K_3h^2 + (EA/2)M_0{}^2K_4h^2 + \\ &EAM_0K_5h^2 + (EA/2)K_6h^{5/2} + (EA/2)M_0K_7h^{5/2} + (EA/8)K_8h^3\end{aligned} \tag{15}$$

where in Eq. (15), $K_1, \ldots, K_8$ are constants independent of h. Clearly as $h \to 0$, $|\varepsilon| \to 0$.

Conclusions

When nonlinear effects are large, the constants K_i, $i \geqq 3$, appearing in Eq. (15) may be on the order of those obtained in error estimates for the linearized problem. Clearly, the use of cruder approximations for $\eta'(x)$ governs the rate-of-convergence of the model. Had cubic approximations been used throughout, we would have obtained $|\varepsilon| = O(h^4)$ for h sufficiently small; for the mixed problem, $|\varepsilon| = O(h^2)$. However, this still may be an acceptable rate of convergence, particularly if "mildly nonlinear" behavior is evident.

We remark that the use of simpler functions for such terms may well be justified in more complicated problems like plate and shell bending problems. In a typical nonlinear analysis where usually an iterative or a step by step method may be required to solve Eqs. (6a) and (6b), the terms $\mathbf{Q}_1$, $\mathbf{Q}_2$, and $\mathbf{Q}_3$ due to nonlinear effects need be calculated several times, so their calculations take major part of the solution effort. Simpler functions may avoid numerical integration of these terms and this may result with significant savings in computational efforts. However, a larger number of elements is required in an inconsistent model to obtain comparable accuracy.

References

[1] Oden, J. T., "Calculation of Geometric Stiffness Matrices for Stability Analysis of Complex Structures," *AIAA Journal*, Vol. 4, No. 8, Aug. 1966, pp. 1480–1482.

[2] Argyris, J. H., Kelsey, S., and Kamel, H., "Matrix Methods of Structural Analysis: A Précis of Recent Developments," *Matrix Methods of Structural Analysis*, AGARDograph 72, Pergamon Press, Oxford, England, 1964.

[3] Oden, J. T., *Finite Elements of Nonlinear Continua*, McGraw-Hill, New York, 1972.

[4] Schultz, M. and Varga, R. S., "L-Splines," *Numeriche Mathematik*, Vol. 10, No. 19, 1967.

A Graphical Method for the Investigation of Shock Interference Phenomena

DAVIS H. CRAWFORD*
NASA Langley Research Center, Hampton, Va.

A NUMBER of recent studies of shock interference have been directed toward correlation and interpretation of local flow phenomena with special emphasis on the prediction of local heating rates.[1] Although the pressure-deflection-shock polar method of determining simple shock interference flowfields has been in hand many years,[2,3] the method is unwieldy and has never found wide acceptance as a design tool. Edney demonstrated its application to several relatively complex interference patterns[4] but his more recent work as well as that of others relies on machine programs which require access to sophisticated computers and are used successfully only after extensive experience by the operator.[5,6] Although the shock polar method lacks the arithmetic precision of the computer,

Received June 4, 1973.
Index categories: Supersonic and Hypersonic Flow; LV/M Aerodynamics; LV/M Configurational Design.

* Aerospace Engineer. Member AIAA.

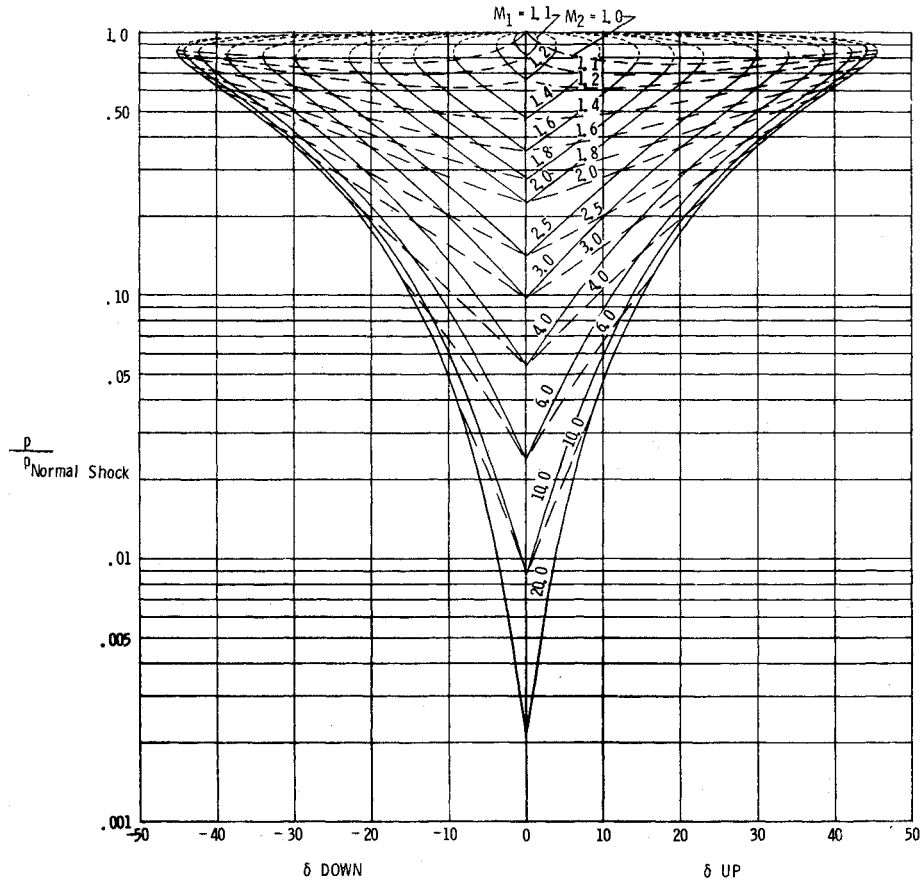

Fig. 1 Logarithmic-shock-polar family.

it can provide a useful tool for students and others searching for trends of shock interference phenomena, and has added advantages in the physical interpretation of the results.

The basic difficulty in using the conventional shock-polar diagrams stems from the necessity to iterate every solution from an infinite family of curves. This difficulty is completely overcome by plotting the pressure-deflection diagrams with the pressure ratio on a logarithmic scale and the deflection on a linear scale. Since any ratio is represented by a certain fixed physical dimension on a logarithmic scale, the polar for a given Mach number is uniquely defined on this set of coordinates. Thus, if a family of polar diagrams is plotted for various Mach numbers so that the polar diagram for any Mach number can be estimated by interpolation, a complicated shock-interference pattern can be hypothesized without a single calculation by tracing the polars from the logarithmic-shock-polar family.

A convenient form for such a logarithmic-shock-polar family is shown in Fig. 1. The polars are aligned so that they are all tangent at the top. The part of each polar representing a weak shock (attached) is a solid line, while the part representing a strong shock (detached) is a dotted line. Since every point on each polar represents a different downstream Mach number, the points representing a given downstream Mach number on the polars can be connected to form an envelope (dashed lines) of constant downstream Mach number. The scale pressure is nondimensionalized with respect to the static pressure behind a normal shock, P_{ns}, and thus reaches a maximum of 1.00 at the top.

To determine the additional pressure vs deflection caused by a second shock in the initially deflected flow, the second polar must be the proper shape and size for the particular point where it is attached to the first polar. Extending the constant downstream Mach number along the envelope from the attachment point back to the y axis establishes that polar which must be used. The initial polar is keyed to the reference pressure (static pressure behind the normal shock) of the freestream. The ordinate distance of the secondary polar, being on a logarithmic scale, automatically conveys the multiplication of the second shock compression to the initial shock compression, and the final result is nondimensionalized with respect to the initial reference pressure of the freestream.

The use of the log-shock-polar diagram may be demonstrated with the aid of Fig. 2. This is the case of two shocks of opposite families intersecting with a resulting pair of shock reflections from a shear layer. When M_∞ is deflected by wedge δ_1, the initial downstream Mach number is M_1, and likewise with M_∞, δ_2, M_2, respectively. Figure 2b shows how the deflections on the freestream polar give pressure ratioed to the stream pressure behind the normal shock for the freestream flow. The two envelopes representing constant downstream Mach number select the proper polars to be placed on 1 and 2. Figure 2c indicates how both of these polars have been repositioned so that further deflections will give pressure ratioed to the static pressure behind a normal shock of the initial freestream. The intersection of these two polars gives the direction of the shear layer downstream of the shock intersection and the common pressure ratio on both sides of this shear layer.

The use of the pressure behind the freestream normal shock, as the reference pressure in complex situations, can be seen more clearly if one considers the flow over a double wedge as represented in the polar diagram of Fig. 3. The ordinate distance between the points 1 and 2 represents the ratio of the scale values of the ordinate since the ordinate is laid off in a logarithmic scale. Projecting back along a constant downstream Mach number curve from 2 to 3, the polar describing the deflection δ_2 for the downstream Mach number at 2 is identified. The ordinate distance between 3 and 4 is the ratio of the ordinate values. When the polar from 3 is transferred to 2, the ordinate values are added or the ratios are multiplied together. In other words

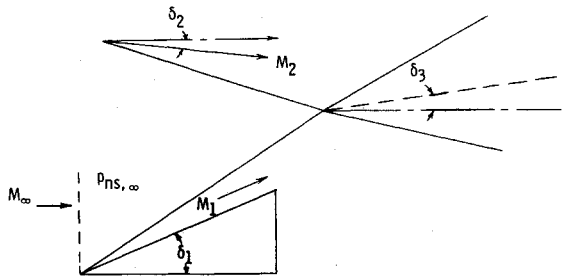

a) Type of interaction calculated.

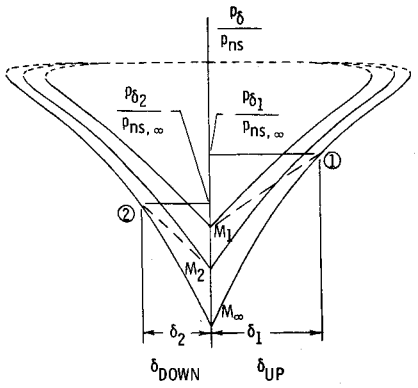

b) Parts of "Logarithmic-Shock-Polar" used.

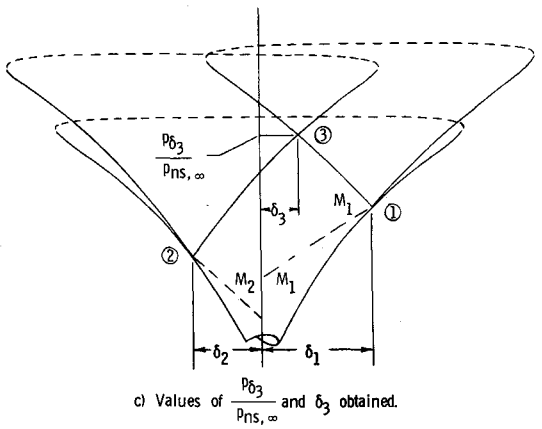

c) Values of $\frac{p_{\delta 3}}{p_{ns,\infty}}$ and δ_3 obtained.

Fig. 2 Example of use of logarithmic-shock-polar diagram.

$$\left(\frac{P_\infty}{P_{ns,\infty}}\right)\left(\frac{\frac{P_1}{P_{ns,\infty}}}{\frac{P_\infty}{P_{ns,\infty}}}\right)\left(\frac{\frac{P_2}{P_{ns,\infty}}}{\frac{P_1}{P_{ns,\infty}}}\right)=\left(\frac{P_\infty}{P_{ns,\infty}}\right)\left(\frac{P_1}{P_\infty}\right)\left(\frac{P_2}{P_1}\right)=\left(\frac{P_2}{P_{ns,\infty}}\right)$$

The value of the logarithmic-shock-polar diagram has been illustrated by its use in two examples, one of which could have necessitated the use of iteration, and one which did not. It can be further utilized to evaluate the two types of three-shock-configuration[2] encountered in shock interaction, i.e., weak oblique wave striking a strong shock, and a weak oblique wave striking another oblique wave of the same family. Both of these have the necessary contact discontinuity line,[2] the first in the form of a shear layer, and the second in the form of an expansion wave. The logarithmic-shock-polar family can be used to estimate the results of reflections from shock waves and expansion waves from a solid wall, or from a free shear layer. These represent all the uses of shock interaction at a point necessary to explain any of Edney's six distinct types of shock

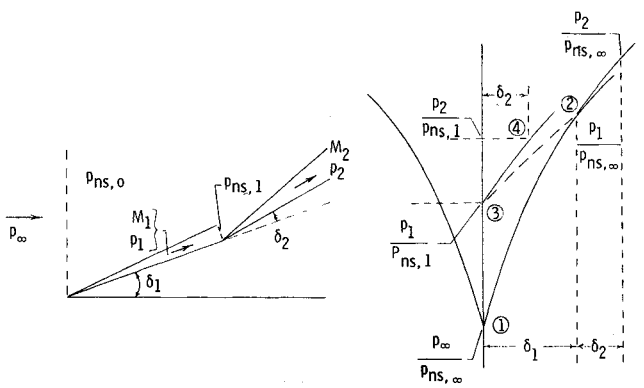

a) Flow over double wedge. b) "Logarithmic-Shock-Polar" for flow over double wedge.

Fig. 3 Another use of logarithmic-shock-polar diagram.

interference pattern. Thus, the pressure-deflection-shock-polar presented in a semilogarithmic format becomes an effective design tool, uniquely applicable to the estimation of multiple shock interference patterns and the resulting pressure changes on affected surfaces.

References

[1] Keyes, J. W. and Hains, F. D., "Analytic and Experimental Studies of Shock Interference Heating in Hypersonic Flows," TN D7139, 1973, NASA.

[2] Courant, R. and Friedrichs, K. O., *Supersonic Flow and Shock Waves*, Interscience Publishers, New York, 1948.

[3] Shapiro, A. H., *The Dynamics and Thermodynamics of Compressible Fluid Flow*, Ronald Press, New York, 1953.

[4] Edney, B. E., "Anomalous Heat Transfer and Pressure Distribution on Blunt Bodies at Hypersonic Speeds in the Presence of an Impinging Shock," FFA Rept. 115, Feb. 1968, The Aeronautical Institute of Sweden, Sweden.

[5] Edney, B. E., Keyes, J. W., Bramlette, T. T., Ives, J., and Hains, F. D., "Theoretical and Experimental Studies of Shock Interference Heating," Rept. 9500-920-195, Oct. 1970, Bell Aerospace Co., Buffalo, N.Y.

[6] Edney, B. E., "Shock Interference Heating and the Space Shuttle," TM X-52876, Vol. 1, July 15–17, 1970, NASA.

[7] "Equations, Tables, and Charts for Compressible Flow," Rept 1135, 1953, NACA.

Calculation of Turbulent Boundary-Layer Shock-Wave Interaction

DAVID C. WILCOX*
Applied Theory Inc., Los Angeles, Calif.

IN the past few years phenomenological turbulence model equations have been applied to increasingly more difficult turbulent flowfield problems. Most complex fields can be solved

Received May 29, 1973. J. G. Trulio of Applied Theory Inc. and P. G. Saffman of the California Institute of Technology provided valuable guidance and assistance during the course of this study. Research was sponsored by the Air Force Aerospace Research Laboratories, Air Force Systems Command, United States Air Force, Contract F33615-72-C-1780.

Index categories: Boundary Layers and Convective Heat Transfer—Turbulent; Jets, Wakes and Viscid-Inviscid Flow Interactions.

* Staff Scientist; presently affiliated with DCW Industries, Sherman Oaks, Calif. Member AIAA.